Fuel Processing Technology 262 (2024) 108113

Contents lists available at ScienceDirect

Fuel Processing Technology

journal homepage: www.elsevier.com/locate/fuproc

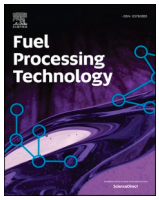

Effect of raw material, moisture and high-temperature tertiary air on a coal gasifier for cement precalciation

Zhang Leyu [a,b], Chen Qingqing [a,b], Wei Xiaolin [a,b,*], Cheng Heng [a], Li Sen [a,b]

[a] State Key Laboratory of High Temperature Gas Dynamics, Institute of Mechanics, Chinese Academy of Sciences, Beijing 100190, China
[b] School of Engineering Science, University of Chinese Academy of Science, Beijing 100049, China

ARTICLE INFO

Keywords:
Pulverized coal gasification
High-temperature tertiary air
NO_x reduction
Cement precalciner

ABSTRACT

This paper proposes a new method of pulverized coal gasification using high-temperature tertiary air in a cement precalciner, in which an external hanging gasifier is added nearby. A full-scale model is established and simulated for the entrained flow gasifier. During the gasification process, the global reaction mechanism is used to model the release and reactions of volatiles from pulverized coal, and a particle surface reaction model is employed to calculate the fixed carbon content. The mechanism by which reducing gas reacts with NO is also considered. The results of the velocity, temperature, gas composition, NO_x emissions, calorific value, volatile conversion ratio and char burnout ratio, are achieved in the simulation. The results show that the volatile conversion ratios were close to 100%, and the carbon conversion ratios ranged from 27.97% to 62.76% among all the tested conditions. The concentrations of NO at the outlet of the gasifier were 109, 98, 75, 91, 87, 76, and 90 mg/m^3 separately in 7 conditions. These values are significantly lower than those of complete combustion. However, the addition of raw meal had the best temperature control effect, leading to a significant decrease in thermal NO_x production and no side effects on the stability of the production line.

1. Introduction

As an important raw material in China's infrastructure, more than 2 billion tons of cement are produced per year, accounting for about half of the world's total production [1]. There are more than 2000 new dry process cement production lines in China. Although the cement industry has contributed to much of the infrastructure construction in China, its use continues to be hindered by the defects of high energy consumption and high pollution. The precalciner, with 60% of total coal consumption in the cement production line, is one of the most important pieces of equipment in the cement production process. The precalciner simultaneously performs pulverized coal combustion and raw material decomposition reactions. Due to the presence of high temperature in the furnace, some N_2 in the furnace is transformed into thermal-NO_x [2,3], and the nitrogen contained in the pulverized coal is also transformed into fuel-NO_x [4,5]. According to statistics, the cement industry emits more than 18 million tons of NO_x pollutants annually, and the removal of NO_x pollutants greatly increases the subsequent treatment costs. To achieve ultra-low NO_x emissions (50 mg/Nm^3), SCR needs to be applied to reduce NO_x next to the sprayers of SNCR that are installed in the top of precalciner.

Currently, selective non-catalytic reduction (SNCR) [6] is widely used in the cement industry for denitrification, using urea solution or ammonia solution as a reducing agent to react with NO in flue gas and reduce it to N_2. Since the efficiency of the SNCR method is only about 50%–65%, the unreacted ammonia is discharged into the atmosphere with the flue gas, resulting in the fugitive ammonia phenomenon. In addition, the SNCR method has the disadvantages of high reducing agent consumption and high operating costs. In some specific regions of the country with the most stringent pollutant emission standards, a few cement plants have attempted to use selective catalytic reduction (SCR) [7] for pollutant removal, which produces frequent catalyst poisoning and high operation and maintenance costs. While SCR employs catalysts to achieve denitrification efficiency of over 85% in contrast to SNCR, it is important to consider the associated challenges such as the substantial initial investment costs, frequent catalyst poisoning, and high operation and maintenance costs. With the increasing focus on environmental protection and the imperative of energy conservation and emission reduction, the cement industry is in urgent need of new processes and methods to improve production efficiency and reduce pollutant emissions.

Coal gasification is mainly divided into three categories: fixed bed,

* Corresponding author at: State Key Laboratory of High Temperature Gas Dynamics, Institute of Mechanics, Chinese Academy of Sciences, Beijing 100190, China
E-mail address: xlwei@imech.ac.cn (W. Xiaolin).

https://doi.org/10.1016/j.fuproc.2024.108113
Received 15 May 2024; Received in revised form 10 July 2024; Accepted 23 July 2024
Available online 5 August 2024

fluidized bed and entrained flow reactor. As a mature technology, coal gasification has achieved industrialized and stable production. Although the entrained flow reactor is a relatively new technology, it enables simple continuous production. This method has the advantages of large working load, high reaction temperature, and strong adaptability to coal type, and has received increasing attention [8]. Considering the fact that pulverized coal pre-gasification in the fuel-rich state can produce abundant reducing gases containing a large amount of CO and H_2, these gases can be fed into the precalciner as a fuel with multiple inlets to reduce NO_x. Since pulverized coal pre-gasification technology is rarely used in cement production lines and field tests are unaffordable in terms of time and cost, the application of computational fluid dynamics (CFD) numerical simulations is becoming more sophisticated and accurate in the engineering analysis of cement kilns [9,10]. Therefore, it is necessary and feasible to carry out the experimental study of pulverized coal gasification and graded combustion technology in cement kilns by using a numerical simulation calculation method based on the above ideas.

In recent years, coal gasification technology in China has undergone continuous and rapid development. The updraft straw gasifier developed by the Institute of Mechanics adopts a design where the gasification agent enters from the bottom while the straw enters from the top, achieving countercurrent movement. Under experimental conditions, this gasifier can produce high heating value gas, with an average carbon conversion rate of 86.4% and a gasification efficiency of up to 73.3% [11]. The dual circulating fluidized bed gasification technology developed by the Institute of Engineering Thermophysics separates the pyrolysis gasification of coal from semicoke combustion through two beds; it utilizes high temperature circulating ash as the heat carrier in the gasifier to obtain high calorific value gas under limited oxygen conditions, while releasing heat through semicoke combustion. By hierarchically converting the active components of coal, the technology enables simultaneous production of heat, gas, and oil, following the principle of energy cascade utilization. Dual bed gasification experiments have shown that the maximum total carbon conversion rate can reach 96.6%, and the combustion efficiency of semicoke can reach 98% [12].

The Tsinghua gasifier is a newly developed oxygen-staged slurry-feed membrane wall gasifier that divides the primary oxygen supply process into the combustion stage and oxygen supplementation stage to ensure that the temperature remains below the ash fusion point and the staged gasification objectives are achieved. The Tsinghua gasifier using coal water slurry has the advantages of lower energy consumption and risk compared to dry powder membrane water wall gasifiers; it can adapt well to different types of coal, including high ash and high sulfur coal. Operating at a lower temperature and with good stability, the Tsinghua gasifier achieves a high carbon conversion rate of up to 98% and approximately 80% effective components in syngas ($CO + H_2$). [13].

KHD Humboldt Wedag developed the PYROCLON® REDOX system, which is characterized by a denitration gasifier between the kiln inlet chamber and calciner for emission reduction. Kiln exhaust gases undergo sub-stoichiometric combustion, creating CO-rich conditions. And then CO reacts with NO_x, reducing them to harmless CO_2 and N_2. The remaining gas undergoes oxidation in the calciner with O_2-rich tertiary air and raw meal, ensuring thorough calcination. PYROCLON® REDOX can achieve a 66% reduction in NO_x emissions when combined with an existing SNCR system in China [14].

In recent years, we proposed a patent titled “A high temperature tertiary air gasification and reburning system for efficient denitration in cement precalciner” (Patent No. CN 107099336 B) [15]. This system utilizes the hot gas as the reburning fuel to reduce NO_x, enabling efficient denitrification and economic efficiency. This invention has the advantage of not requiring the installation of large-scale equipment and minimal investment. In addition, the Institute of Engineering Thermophysics proposed a low NO_x emission control technology using a cement laboratory precalciner with a circulating fluidized bed gasifier [16].

In this study, we investigated the proposed method of pulverized coal gasification using high temperature tertiary air. Fig. 1 shows the system framework of this new method. An external hanging gasifier was added near the precalciner. First, part of the high temperature tertiary air in the cement production line is introduced into the gasifier to react with the pulverized coal. Then, the hot gas is directly carried into the cement precalciner to achieve low NO_x combustion. The exhaust flue gas from the kiln’s exhaust chamber enters the bottom inlet of the cement precalciner. After that, CO reacts with NO_x, reducing them to harmless CO_2 and N_2. For simulation, the pulverized coal gasifier using high temperature tertiary air was simulated by the CFD software for the first time, which is of great theoretical significance and reference value to reduce NO_x emissions in a cement precalciner.

2. CFD and chemical reaction methods

2.1. CFD method

The CFD method (RANS) was used to simulate pulverized coal gasifiers and includes the following models: the realizable k-ε model, species transport model, discrete phase model, discrete random walk model, and radiation model.

The discrete phase model (DPM) [17] was chosen for pulverized coal combustion, 620 pulverized coal particles were tracked, and the particle size distribution was calculated using the Rosin–Rammler distribution. The particle temperature is consistent with the primary air temperature, which is 70 °C.

The discrete ordinates (DO) model [18] was chosen for the radiation heat transfer model, and the weighted-sum-of-gray-gases model (WSGGM) [19] was used to calculate the absorption coefficient of the gas phase.

The control equations of the fluid phase were discretized by the controlling-volume method, and the difference equations were solved by a second-order upwind difference scheme. The SIMPLE algorithm was used to couple the pressure and velocity. The convergence criteria were taken as the residual term of the continuity and energy equations less than 10^{-6} and the residual term of the remaining terms less than 10^{-3}.

The carbon conversion ratio is defined as follows:

$$\text{carbon conversion ratio} = 1 - \frac{\text{mass flow of carbon at the outlet}}{\text{initial mass flow of carbon}}$$

2.2. Chemical reaction model and the NO_x model

Volatile decomposition and reaction were assumed to occur first in the coal gasification process, followed by the reaction of char. The volatile pyrolysis used the two-competing-rates model. The EDC (eddy-dissipation concept) model was used to express the gas turbulent chemical reactions in the gasifier. The reactions of volatile decomposition and gas (R1-R4) are given.

The combustion of char (R5-R7) was modeled using the particle

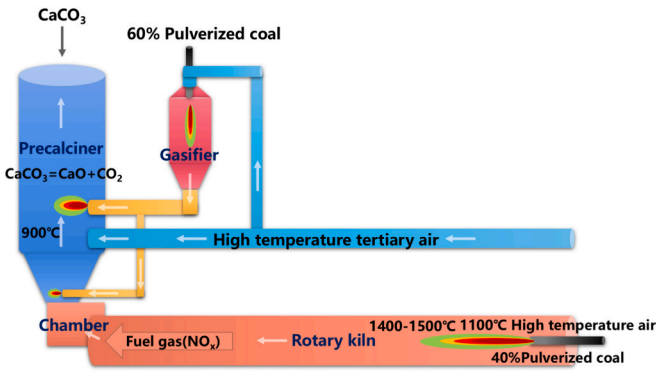

Fig. 1. System schematic.

surface reaction model, in which the first-order Arrhenius model was used.

NO_x can be classified as thermal-NO_x, fuel-NO_x or prompt-NO_x, based on different formation principles. Because thermal NO_x is mainly formed above 1500 °C and the internal temperature of the gasifier can be above 1500 °C, thermal NO_x should be considered. Fuel-NO_x is generated by nitrogen in pulverized coal and is the predominant form of NO_x produced in precalciners. Prompt-NO_x is formed by the prompt reaction of the flame front, which only accounts for a small proportion of the total NO_x, so it is negligible. In addition, the reductive atmosphere of coal gas can react with NO to decrease the emission value, so R8-R10 should be considered.

The probability density function (PDF) model was used to simulate the turbulent interactions in the NO_x model. For fuel-NO_x, the volatile-N reaction intermediates were 90% HCN and 10% NH_3, and the char-N reaction intermediate was NO.

Table 1 shows the reaction mechanism data. R11-R16 are the mechanisms of thermal NO_x, R17-R20 are the mechanisms of volatile NO_x, and R21–24 are the mechanisms of N_2O.

3. Geometrical model and boundary conditions

3.1. Geometrical model

The gasifier is modeled according to the full-scale model (see Fig. 2). The upper inlet is divided into the pulverized coal inlet, steam inlet and tertiary air inlet, and the bottom is the outlet. The height of the furnace is 11,600 mm, and the inner diameter is 3200 mm. The mesh is divided into three parts: the upper throat, middle cylindrical body, and lower throat. A fully structured meshing method is used. The total number of meshes is 722,000, the mesh quality is 0.8, the aspect ratio is 5.877:1, and the minimum orthogonal quality is 0.737, which indicates the mesh quality is good. The high-quality mesh ensures the stability of the subsequent calculations and speeds up the convergence.

The design parameters and operating parameters of the gasifier are shown in Table 2. The operating conditions are shown in Table 3, and the proximate and ultimate analyses of the coal samples are shown in Table 4.

3.2. Mesh independence and validation

3.2.1. Mesh independence

The three sets of grids were used for simulation (see Table 5 and Fig. 3), using the largest grid size of No. 1 as the reference. The calculated values of each point of No. 2 are close to those of No. 1, while the error of No. 3 is relatively large. Considering the computational economy and simulation accuracy, a mesh of 722,000 grids was selected for subsequent calculations.

3.2.2. Data validation

The simulation results of the designed operating conditions are compared with the experimental data, and the results are shown in Table 6. The concentrations of CO, H_2 and CO_2 are all close to those of the experimental data, validating the reliability of the selected mathematical model and the numerical calculation algorithm; this indicates that they are suitable for subsequent calculations.

The field test was run for approximately 1 h and was stopped due to a valve failure, which made it impossible to adjust the valve opening. The volume of tertiary air introduced into the gasifier was even smaller than that in the simulated set under Condition 5 (the excess air coefficient was 0.2), so the degree of coal gasification was lower, and the average outlet temperature was approximately 160 K lower than the simulated value.

Fig. 4 shows the simulated values are smaller than the experimental values, which may be due to the following reasons: During the field test, there was a large amount of air leakage in the duct, resulting in an abnormal operating condition in the gasifier. It was measured that when the air leakage reaches 10%, the average temperature in the gasifier would be reduced by about 150 K, which was consistent with the simulation conclusions. In addition, the environment temperature was low during the test, and the temperature difference caused by the air leakage was further aggravated.

Fig. 5 shows that for Case 4, there is a more obvious cyclonic effect in the gasifier, which can effectively increase the residence time of the material. The high-temperature zone is concentrated in the central part of the gasifier, which has a symmetrical distribution effect along the radial direction, which is conducive to heat protection.

Table 1
Data on the reaction mechanism.

No.	Reaction	*A*	*β*	*E*	Order of reaction	Ref
R1	$C_{1.32}H_{4.15}O_{0.55}N_{0.0758}+ 1.42O_2 \rightarrow 1.32CO + 2.075H_2O + 0.0379\ N_2$	2.12e+11	0	2.03e+08	$[vol]^{0.2}[O_2]^{1.3}$	[20]
R2	$CO + 0.5O_2 \rightarrow CO_2$	2.24e+12	0	1.7e+08	$[CO]^1[O_2]^{0.25}$	[21]
R3	$CO + H_2O \rightarrow CO_2 + H_2$	2.75e+12	0	8.37e+07	$[CO]\ [H_2O]$	[22]
R4	$H_2 + 0.5\ O_2 \rightarrow H_2O$	1.21e+18	−1	1.26e+08	$[H_2]^{0.25}[O_2]^{1.5}$	[22]
R5	$C(s) + 0.5O_2 \rightarrow 0.5CO$	0.005	0	7.4e+07	$[O_2]$	[23]
R6	$C(s) + CO_2 \rightarrow 2CO$	0.00635	0	1.62e+08	$[CO_2]$	[24]
R7	$C(s) + H_2O \rightarrow CO + H_2$	0.00192	0	1.47e+08	$[H_2O]$	[24]
R8	$CO + NO \rightarrow \ldots \rightarrow CO_2 + N_2$	2.14e+05	0	8.37e+07	$[CO]\ [NO]$	[25]
R9	$H_2 + NO \rightarrow \ldots \rightarrow H_2O + N_2$	1.2e+07	0	7.17e+07	$[H_2]\ [NO]$	[25]
R10	$C(s) + NO \rightarrow \ldots \rightarrow CO + N_2$	0.00253	0	1.34e+08	$[NO]^{0.7}$	[26]
R11	$O + N_2 \rightarrow N + NO$	3.19e+08	0	1.8e+08	/	[27]
R12	$N + NO \rightarrow O + N_2$	3.53e+06	0	3.8e+07	/	[28]
R13	$N + O_2 \rightarrow O + NO$	3.89e+07	1	1.8e+04	/	[28]
R14	$O + NO \rightarrow N + O_2$	1.73e+08	1	3.81e+03	/	[28]
R15	$N + OH \rightarrow H + NO$	3.74e+06	0	7.1e+07	/	[28]
R16	$H + NO \rightarrow N + OH$	2.04e+08	0	1.7e+08	/	[28]
R17	$HCN + O_2 \rightarrow NO$	1.0e+10	0	2.80e+08	[HCN]	[29]
R18	$HCN + NO \rightarrow N_2$	3.0e+12	0	2.51e+08	[HCN] [NO]	[29]
R19	$NH_3 + O_2 \rightarrow NO$	4.0e+06	0	1.34e+08	$[NH_3]$	[29]
R20	$NH_3 + NO \rightarrow N_2$	1.8e+08	0	1.13e+08	$[NH_3]\ [NO]$	[29]
R21	$N_2 + O + M \rightarrow N_2O + M$	4.44e+32	−8.358	2.35e+08	/	[30]
R22	$N_2O + M \rightarrow N_2 + O + M$	4.00e+08	0	2.35e+08	/	[30]
R23	$N_2O + O \rightarrow 2NO$	2.90e+07	0	9.69e+07	/	[30]
R24	$2NO \rightarrow N_2O + O$	1.45e-29	9.259	9.69e+07	/	[30]
R25	$CaCO_3 \rightarrow CO_2 + CaO$	5.203e+08	0	2.05e+08	$[CO_2]$	[31]

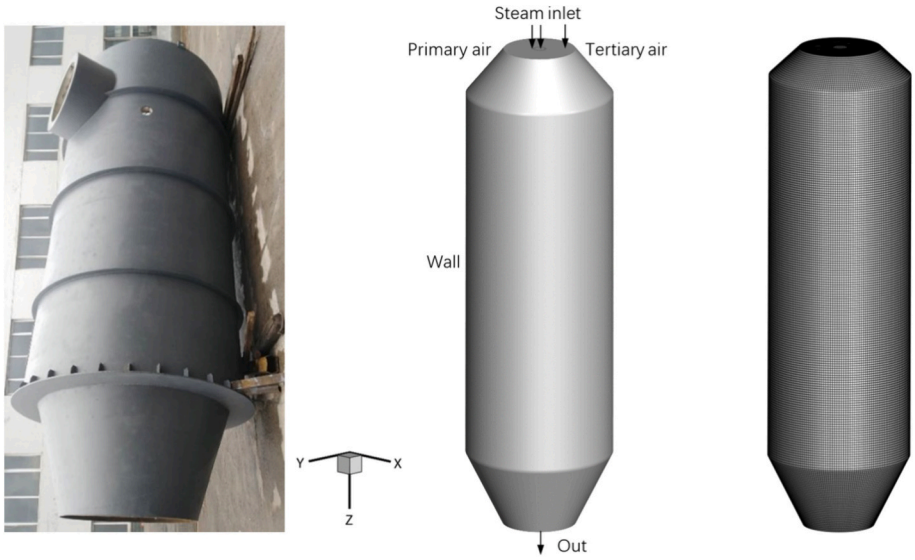

Fig. 2. Gasifier structure and mesh.

Table 2
Design and operation parameters of the gasifier.

Parameter	Value
Height of gasifier	11,600 mm
Diameter of gasifier	3200 mm
Diameter of burner	200/300 mm
Diameter of inlet	1800 mm
Diameter of outlet	1600 mm
Coal feeding rate	12 t/h
Air flow rate of carried coal	2800 Nm^3/h
Flow rate of tertiary air	18,200 Nm^3/h
Temperature of tertiary air	1173 K
Ratio of air to coal	0.53 kg/kg
Steam flow rate	0–1 t/h
Temperature of steam flow rate	598 K
Raw meal flow rate	0–21.6 t/h
Temperature of raw meal	1053 K

Table 3
Operating conditions.

No.	Air temperature (K)	Excess air coefficient	Steam (t/h)	Raw meal (t/h)
1	1173	0.3	0	0
2	1173	0.3	1	0
3	1173	0.3	0	21.6
4	1173	0.2	0	0
5	1173	0.2	1	0
6	1173	0.2	0	21.6
7	300	0.3	0	0

4. Results and discussion

4.1. Gas composition and the heating value

Table 7 and Fig. 6 indicate the data of gas composition and heating value under various conditions. Reduction in the excess air coefficient: The comparison between Case 1 and Case 4 shows that the reduction in the excess air coefficient makes the local fuel-rich atmosphere more obvious. In a reducing atmosphere, the concentrations of CO and H_2 both increase significantly. The concentration of CO increased from 10.41% to 17.92%, and the H_2 concentration increased from 4.78% to 5.50%. An increase in the CO concentration leads to a reduction in CO_2, which decreases from 12.46% to 8.22%. An increase in the CO and H_2 concentrations means that more chemical energy is stored, so the calorific value of the gas phase also increases greatly, from 4651 kJ/Nm^3 to 7081 kJ/Nm^3. Due to the fuel-rich atmosphere in the gasifier, the fixed carbon conversion ratio decreases from 49.15% to 39.42%. When the flow rate of unreacted fixed carbon increased from 2702 kg/h to 3219 kg/h, the gas phase sensible heat decreased. The outlet temperature was reduced from 1927 K to 1563 K. Addition of steam: The comparison between Case 1 and Case 2 shows that the addition of steam shifts the chemical equilibrium of reaction R7 to the positive reaction direction and improves the yields of CO and H_2. The CO concentration increased from 10.41% to 13.82%, and the H_2 concentration increased from 4.78% to 9.68%. The gas phase calorific value increased more significantly from 4651 kJ/Nm^3 to 5584 kJ/Nm^3. The fixed carbon conversion ratio increased from 49.15% to 62.70%. The unreacted fixed carbon flow rate decreased from 2702 kg/h to 1982 kg/h. The heat-absorbing reaction R7 resulted in more chemical energy being stored in CO and H_2, and the outlet temperature decreased from 1927 K to 1831 K, showing less gas-phase sensible heat. Addition of raw material: The comparison between Case 1 and Case 3 shows that the CO_2 concentration greatly increases from 12.46% to 30.61% due to the decomposition of $CaCO_3$, while the

Table 5
Comparison of temperature values from the analysis of grid independence.

No.	Mesh totals	Point 1 (0,0,2)	Point 2 (0,0,6)	Point 3 (0,0,11)
1	958,000	681 K	1327 K	1792 K
2	720,000	676 K	1324 K	1789 K
3	530,000	698 K	1350 K	1825 K

Table 4
Data from the coal analysis.

Proximate analysis-%				Ultimate analysis-%					$Q_{net,ar}$
M_{ar}	A_{ar}	V_{ar}	FC_{ar}	C_{ar}	H_{ar}	S_{ar}	N_{ar}	O_{ar}	MJ/kg
9.39	24.79	23.97	41.85	53.97	3.31	0.74	0.84	6.96	20.95

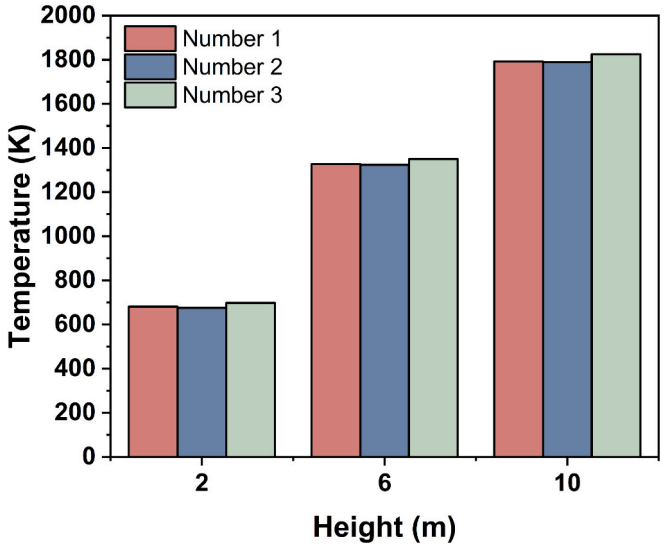

Fig. 3. Temperatures simulated by various grids.

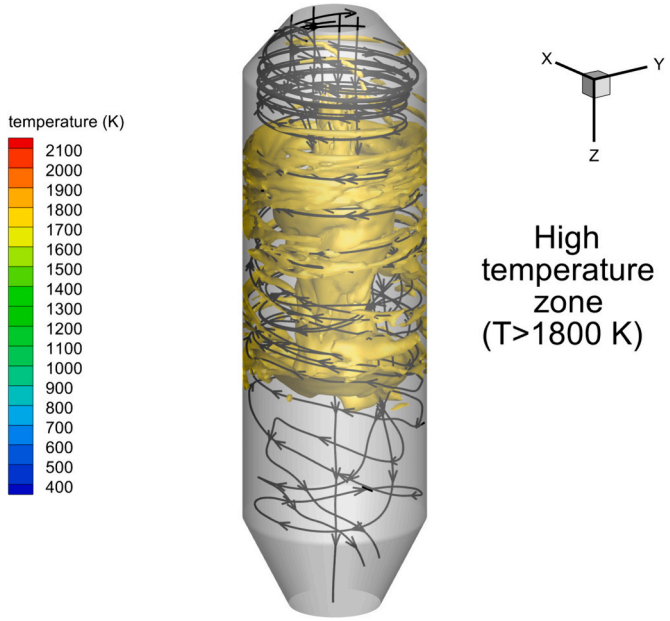

Fig. 5. Streamtraces and the high-temperature zone in the gasifier.

Table 6
Gas composition under condition 2.

Gas composition	1173 K air molar fraction %	Test data [32]
CO	13.82	17
H_2	9.68	11
CO_2	12.37	10
N_2	58.45	54

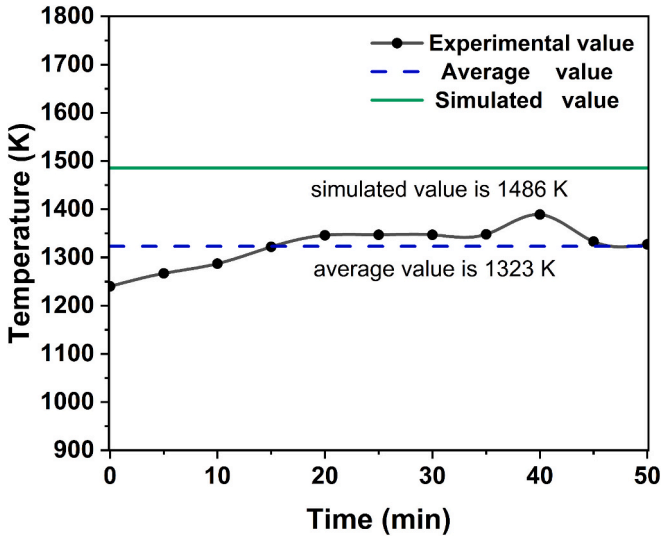

Fig. 4. Validation between the experimental data and simulated data.

heat-absorbing reaction R25 leads to a significant decrease in the outlet temperature from 1927 K to 1349 K and in the gas phase sensible heat. The fixed carbon conversion ratio is significantly reduced from 49.15% to 37.37%. The flow rate of unreacted fixed carbon increased from 2702 kg/h to 3328 kg/h. A decrease in the fixed carbon conversion rate also led to a significant decrease in the gas phase calorific value from 4651 kJ/Nm^3 to 2697 kJ/Nm^3. The heat-absorbing reactions R6 and R7 are inhibited. The CO concentration decreased from 10.41% to 4.20%, and the concentration of H_2 increased from 4.78% to 5.57%, which did not change significantly. Reduction of the tertiary air temperature: The comparison between Case 1 and Case 7 shows that the higher the temperature in the gasifier is, the more the exothermic reaction is suppressed and the more heat-absorbing reactions are carried out, so the yields of CO and H_2 increase. The concentration of CO increased from 10.41% to 13.77%, and the concentration of H_2 increased from 4.78% to 6.24%, which significantly increased the gas phase calorific value from 4651 kJ/Nm^3 to 5348 kJ/Nm^3. The fixed carbon conversion ratio increased from 49.15% to 55.01%, and the flow rate of unreacted fixed carbon decreased from 2702 kg/h to 2392 kg/h. A decrease in the tertiary air temperature led to a decrease in the total enthalpy, and the outlet temperature decreased from 1927 K to 1565 K under a similar reaction process.

4.2. *Effect of the excess air coefficient on gas composition*

As is shown in Fig. 7, H_2 was mainly generated from reaction R7, in which C(s) reacted with H_2O, followed by reaction R3, in which CO reacted with H_2O. However, only a small amount of H_2O is generated from pulverized coal in both Case 1 and Case 4. The concentration of H_2O, as an equilibrium controlling factor, determines the low concentration of H_2. The concentrations of H_2 at the outlet are 4.78% and 5.50%, respectively. Due to the lower excess air coefficient of Case 4, the volatiles are pyrolyzed completely, while the fixed carbon conversion ratio is low. The fixed carbon conversion ratio of Case 4 is even lower than that of Case 1. The fixed carbon conversions are 49.15% and 39.42%, respectively. Both conditions show an obvious local fuel-rich atmosphere in the gasifier. The change in the excess air coefficient affects the temperature and velocity distribution in the gasifier. From the contour data in the figure, the H_2 concentration of Case 4 reaches 5% at a distance of 6.5 m along the gasifier, whereas that of Case 1 reaches 5% at a distance of 8 m along the gasifier. However, the residence times under both conditions are close to each other, which means that the reaction processes are similar.

CO is generated mainly from volatile reaction R1 and reaction R6, in which fixed carbon reacts with CO_2, followed by reaction R7, in which fixed carbon reacts with H_2O. Like the characteristics of the H_2 distribution, the CO distribution is also affected by the change in the excess air coefficient. The distance along the gasifier is greater in Case 1 than in Case 4 at a similar residence time when the same concentration is reached. The distribution of CO in Case 1 shows rapid enrichment and a sharp exit from the outlet, while there is gradual enrichment in Case 4,

Table 7
Gas compositions and heating value under various conditions.

	Mole fraction of CO	Mole fraction of H_2	Mole fraction of CO_2	Mole fraction of N_2	Gas heating value (kJ/Nm^3)	Char flow rate (kg/h)	T_{out} (K)
Case 1	10.41	4.78	12.46	64.49	4651	2702	1927
Case 2	13.82	9.68	12.37	58.45	5584	1982	1831
Case 3	4.2	5.57	30.61	56.06	2697	3328	1349
Case 4	17.92	5.50	8.22	57.62	7081	3219	1563
Case 5	14.69	10.31	11.49	53.81	7729	2543	1486
Case 6	0.72	2.90	36.28	51.72	4516	3834	1108
Case 7	13.77	6.24	12.3	61.63	5348	2392	1565

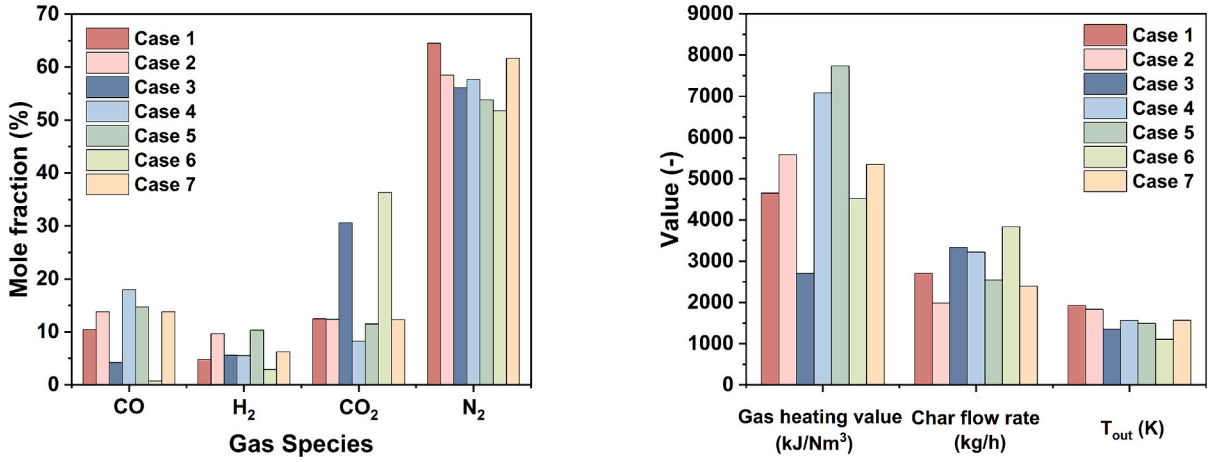

Fig. 6. Data of fuel gas under various conditions.

and the contour of CO is sparser than that in Case 1. The CO concentrations at the outlet are 10.41% and 17.92%, respectively.

The primary air introduces pulverized coal into the gasifier via the upper central inlet. In the central zone of the gasifier, a local fuel-rich atmosphere is formed, where oxygen is rapidly depleted due to the pyrolysis of volatiles. The tertiary air inlet introduces a larger volume of air into the gasifier than does the primary air inlet, and the velocities of the tertiary air inlet and primary air inlet are only approximately half: 10.64 m/s and 20.57 m/s, respectively. The O_2 carried by tertiary air decays more slowly than that carried by primary air. The oxygen is depleted at a distance of approximately 10 m along the gasifier in Case 1 with an excess air coefficient of 0.3, while the oxygen is depleted at a distance of approximately 6.5 m along the gasifier in Case 4 with an excess air coefficient of 0.2. A lower air volume results in a lower amount of available O_2 and quicker O_2 depletion. The oxygen concentrations at the outlet are 0.39% and 0.01%, respectively, indicating that the oxygen in Case 1 is mostly depleted, while the oxygen in Case 4 is completely depleted. A high-temperature zone is formed where oxygen is consumed sharply and shows obvious symmetrical distribution characteristics. The reduction in the excess air coefficient obviously reduces the temperature peak and moves the high-temperature zone from near the lower outlet to the middle of the gasifier, which protects the internal materials of the gasifier to some extent. The excess air coefficient can be used as one of the means to control the temperature in the gasifier.

The peak NO concentrations are only 240–270 mg/m^3 under both conditions, which is significantly lower than the 800–900 mg/m^3 observed under normal conditions (as shown in our previous results [33]). From the contour data in the figure, it can be seen that the peak concentrations of NO all occurred in the high-temperature zone, showing good consistency and prediction accuracy of the simulation. The velocity distribution in Case 4 is low, which indicates a complete NO formation-enrichment-reduction process. Pulverized coal enters the gasifier from the upper inlet and releases NO by volatile pyrolysis. The temperature of the main combustion zone gradually reaches the peak temperature, and thermal NO_x gradually forms the dominant concentration, which is superimposed on fuel NO_x to reach the peak concentration of NO. In the reducing atmosphere of the gasifier, NO is reduced by reacting with H_2 and CO, and the concentration gradually decreases. The NO concentration at the outlet in Case 4 was 91 mg/m^3. Due to the higher velocity in Case 1, the NO concentration only shows a formation-enrichment process and leaves a lower outlet with the fuel gas. The NO reduction process is not manifested, so the process is incomplete compared with that of Case 4. The NO concentration at the outlet in Case 1 is higher than that in Case 4, which is 109 mg/m^3.

4.3. *Effect of adding steam*

As is shown in Fig. 8, H_2O is generated from the pyrolysis of volatiles. The enrichment process of H_2 is slow due to the low concentration of H_2O, which is the controlling factor of the H_2 generation reaction R7. The steam inlet temperature of Case 2 is 598 K, which is higher than the primary air temperature of Case 1 (323*K*). Therefore, the residence time required for volatile preheating is shorter. The high-temperature zone is formed in the lower part of the gasifier near the outlet in Case 1 compared to Case 2, where a higher position of the high-temperature zone appears. The introduction of steam in Case 2 significantly increases the concentrations of H_2 and CO compared to those in Case 1. Since reaction R7 is a heat-absorbing process, the sensible heat of the fuel gas is partially utilized and converted into the internal energy of CO and H_2; therefore, the temperature of the fuel gas at the outlet is slightly reduced. The temperature of Case 1 at the outlet is 1927 K, while the temperature of Case 2 at the outlet is 1831 K. The concentration of H_2 at the outlet in Case 1 is 4.78%, while for Case 2, the addition of steam promotes the conversion of fixed carbon to CO and H_2, and the concentration of H_2 is significantly increased to 9.68% at the outlet. In addition, the addition of steam increased the fixed carbon conversion ratio from 49.15% to 62.70%, and the flow rate of unreacted fixed carbon decreased from 2702 kg/h to 1982 kg/h. The CO concentration is also affected by volatile pyrolysis in reaction R1, so reaction R7 has less of an effect on the CO concentration than on the H_2 concentration. The

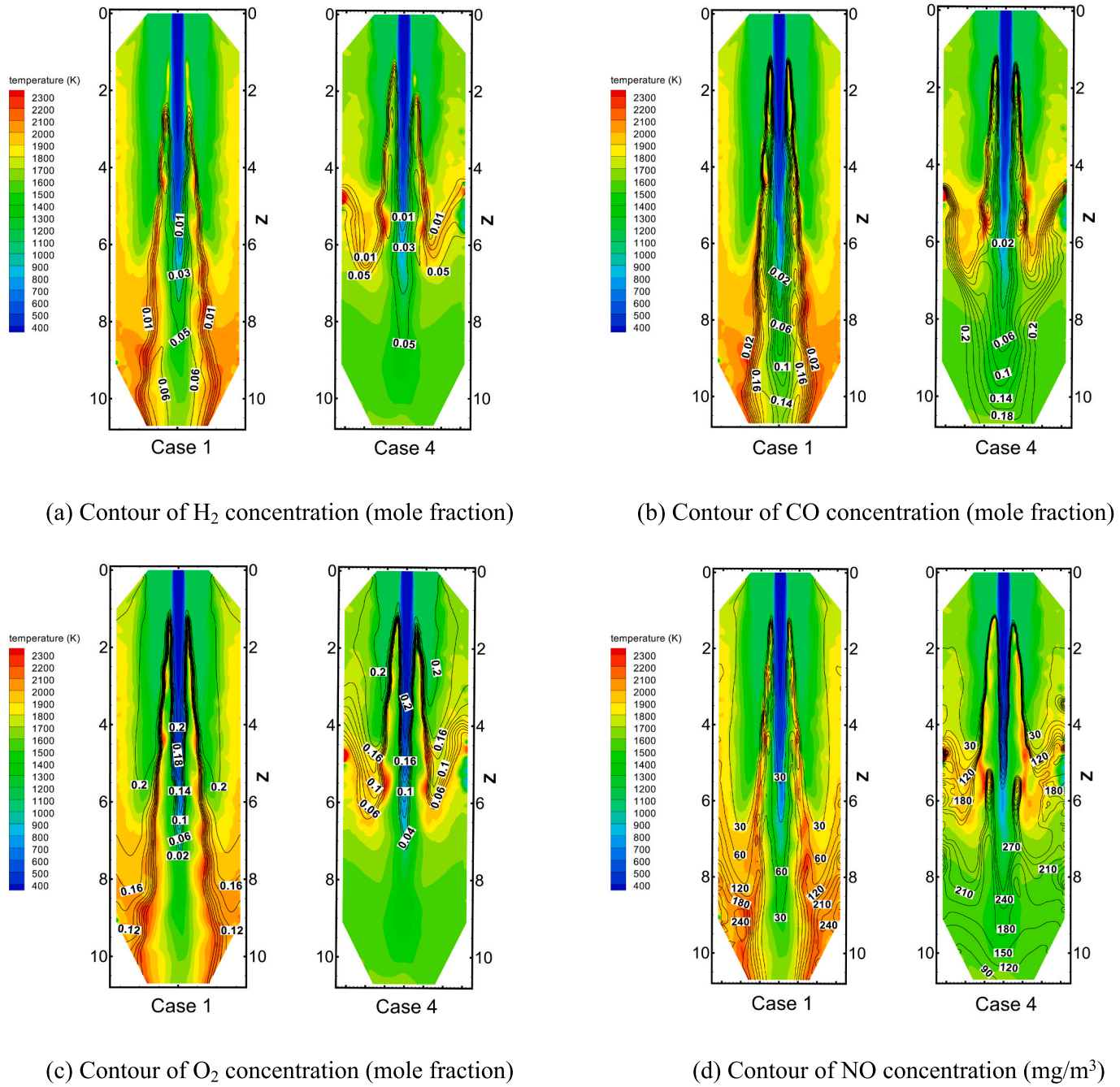

(a) Contour of H_2 concentration (mole fraction)

(b) Contour of CO concentration (mole fraction)

(c) Contour of O_2 concentration (mole fraction)

(d) Contour of NO concentration (mg/m^3)

Fig. 7. Contours of gas composition depicted on the field of temperatures for Case 1 and Case 4.

CO concentration at the outlet increases from 10.41% in Case 1 to 13.82% in Case 2. An increase in the H_2 concentration effectively increased the gas phase calorific value from 4651 kJ/Nm^3 in Case 1 to 5584 kJ/Nm^3 in Case 2.

The O_2 in the primary air is depleted around the inlet in Case 1, while more heat is introduced into the gasifier due to the high-temperature steam inlet in Case 2. The volatiles of pulverized coal are detected and pyrolyzed earlier, and O_2 decays faster. An increase in the temperature of the gasifier accelerates the reaction and promotes the conversion of volatiles to fixed carbon. As the pyrolysis of volatiles and the conversion of fixed carbon from pulverized coal are both exothermic reactions, the heat released promotes an increase in temperature, resulting in a positive cycle. The temperature peak appears earlier than that in Case 1. Since the reaction R7 between fixed carbon and steam is a heat-absorbing reaction, after the temperature peak is reached in Case 2, the sensible heat of the fuel gas is partially utilized and converted into the internal energy of CO and H_2, so the temperature at the outlet decreases. The O_2 concentrations at the outlet are 0.39% and 0.01%, respectively, which are both close to the total depletion. The addition of steam shifts the temperature peak from near the lower outlet to the middle part of the gasifier. The high-temperature zone in Case 2 is far from the wall compared to that in Case 1, so the addition of steam avoids the damage of high temperature to the inner wall materials in the gasifier; therefore, the addition of steam can be used as one of the means to control the temperature in the gasifier.

The addition of high-temperature steam did not have a significant effect on the overall temperature distribution in the gasifier, and only a small difference was observed at the outlet. The NO concentrations are relatively consistent in both cases, with a peak concentration of 240 mg/m^3. Due to the presence of high-temperature steam, the temperature

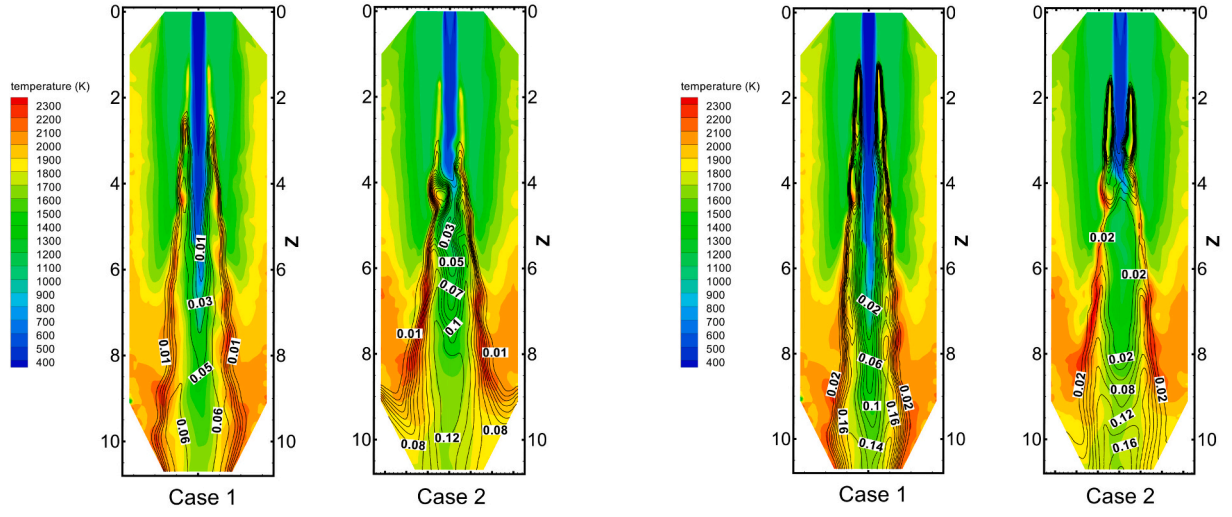

(a) Contour of H_2 concentration (mole fraction)

(b) Contour of CO concentration (mole fraction)

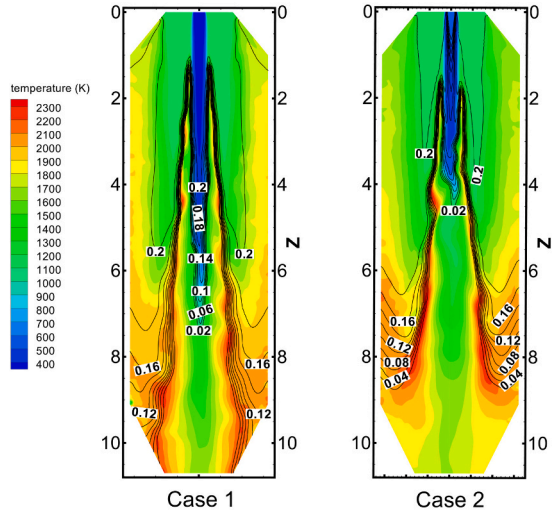

(c) Contour of O_2 concentration (mole fraction)

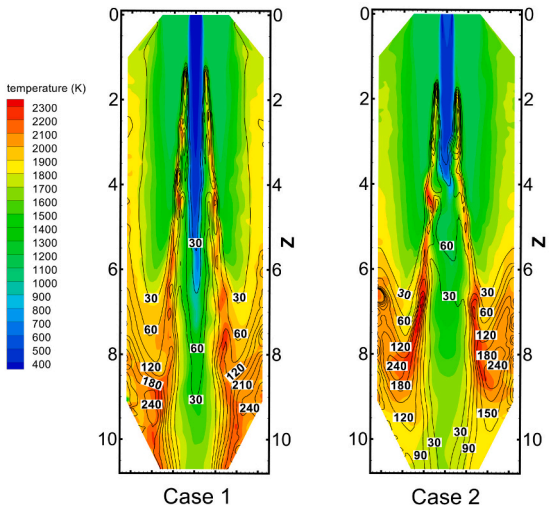

(d) Contour of NO concentration (mg/m^3)

Fig. 8. Contours of gas composition depicted on the field of temperatures for Case 1 and Case 2.

peak occurs earlier and shows a more complete process of NO formation-enrichment-reduction in Case 2 (similar to Case 4). With the presence of more H_2 and CO in Case 2, the ratio of reduced NO increases at the outlet. The concentration of NO is 98 mg/m^3 at the outlet in Case 2, which is lower than the 109 mg/m^3 NO concentration in Case 1.

4.4. *Effect of feeding raw meal*

As is shown in Fig. 9, a comparison between Case 3 and Case 1 shows that when the raw meal is decomposed by heat absorption, the decomposition ratio of $CaCO_3$ reaches 99.37%, which is close to that of complete decomposition. The full decomposition of $CaCO_3$ absorbs a large amount of heat, which greatly reduces the temperature, and there is no obvious temperature peak zone in the gasifier. A lower temperature in the gasifier also slows the reaction of volatile pyrolysis and the conversion of fixed carbon from pulverized coal. The large amount of CO_2 produced by the decomposition of raw meal increases its proportion of the fuel gas, resulting in a significant decrease in the reaction rate of volatile and fixed carbon due to the decrease in temperature. A significant decrease in the consumption rate of O_2 occurred near the central zone. The O_2 concentration is still 14% at a distance of 8 m and 2% at a distance of 10 m along the gasifier. The O_2 consumption rate increases between 8 m and 10 m along the gasifier, indicating that the conversion ratios of volatile and fixed carbon are improved under a longer residence time. The O_2 is almost completely depleted near the lower outlet, and the concentration is only 0.01% at the outlet. In Case 1, the O_2 concentration is 2% in the central zone at a distance of 7.5 m from the gasifier and 0.39% at the lower outlet.

In Case 3, due to the decomposition of the raw meal, there is no significant temperature peak zone in the gasifier. The temperature level in the gasifier is more even and lower than that in the case where no raw meal is added. The temperature slowly increased from the tertiary air inlet of 1170 K to the lower outlet of approximately 1350 K. The thermal NO_x generated was greatly reduced in this temperature range, and the peak NO concentration was only 105 mg/m^3, which is more than half of that in Case 1. The NO concentration at the outlet in Case 3 is only 76 mg/m^3, which is also greatly lower than the value of 109 mg/m^3 in Case 1. The addition of raw meal can be used as one of the means to control

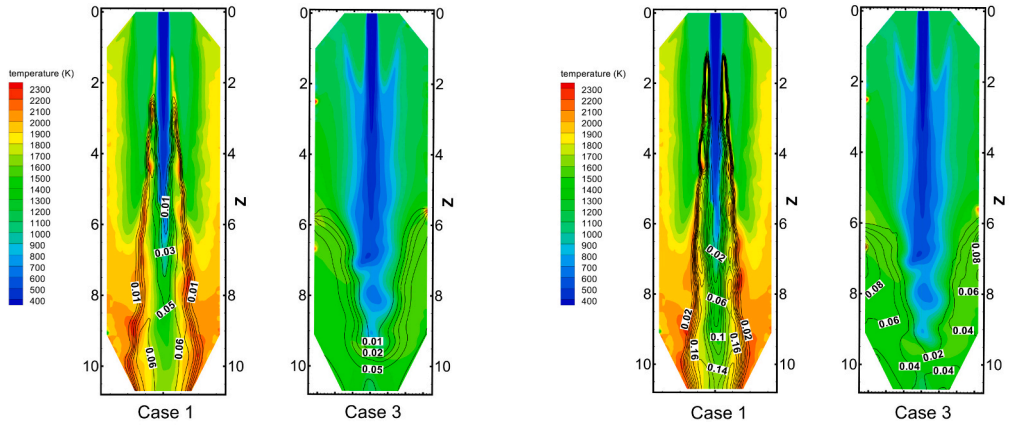

(a) Contour of H_2 concentration (mole fraction)

(b) Contour of CO concentration (mole fraction)

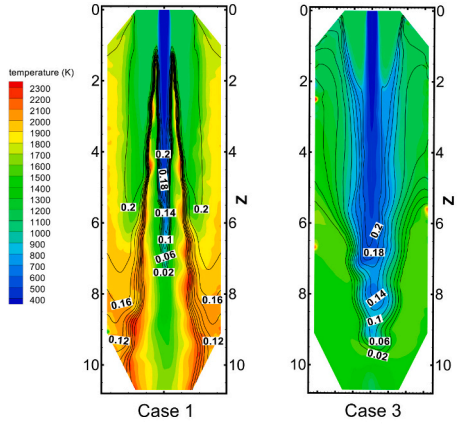

(c) Contour of O_2 concentration (mole fraction)

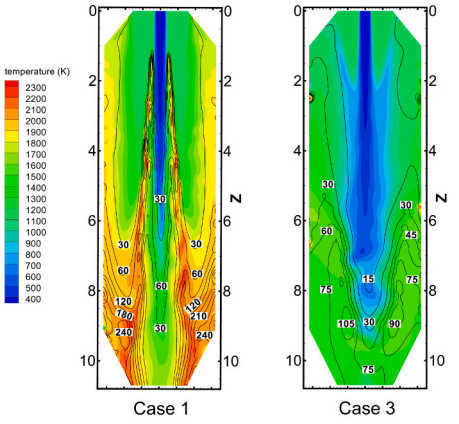

(d) Contour of NO concentration (mg/m^3)

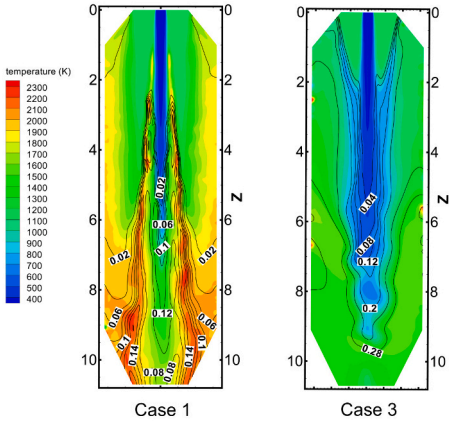

(e) Contour of CO_2 concentration (mole fraction)

Fig. 9. Contours of gas composition depicted on the field of temperatures for Case 1 and Case 3.

the temperature in the gasifier. The addition of raw meal only changes local heat absorption in some zones without affecting the overall heat balance. The stability of daily production is guaranteed because no additional material is introduced into the gasifier. The addition of raw meal can not only be an important means to control the temperature in the gasifier but can also reduce the NO_x concentration and protect the inner material from overheating.

The temperature of the tertiary air is 1170 K, which meets the requirement for the decomposition of the raw meal. The raw meal decomposes rapidly by heat absorption after being introduced into the furnace, which leads to a rapid temperature reduction in the central zone. The zone of temperature below 800 K extends from the upper inlet of the gasifier to a distance of 9 m along the gasifier, and the lateral range is also greatly expanded. The decrease in temperature in the central zone obviously inhibits the pyrolysis of volatiles and the conversion of fixed carbon, and the enrichment of H_2 and CO is also inhibited. The conversion ratios of volatile and fixed carbon are very low. Because the large amount of CO_2 generated accelerates the local

velocity, the residence time of pulverized coal decreases. At the same time, the concentration of CO_2 generated by the decomposition of the raw meal has a high proportion in the fuel gas, which greatly decreases the concentration of H_2 and CO. The CO concentration in Case 3 is less than half of that in Case 1 at the outlet, while the changes in H_2 concentration are not obvious. This indicates that volatile pyrolysis is more complete, and reaction R7 is carried out more completely, which is beneficial to the concentration of H_2. Reactions R5 and R6 are inhibited, so the concentration of CO is greatly affected.

The decomposition of the raw meal is almost complete, so the temperature at the outlet decreases from 1927 K to 1349 K, and the sensible heat of the fuel gas is also greatly reduced. The low temperature in the gasifier slows the pyrolysis of volatiles and the conversion of fixed carbon. The conversion ratio of fixed carbon at the outlet greatly decreased from 49.15% to 37.37%. When the flow rate of unreacted fixed carbon increased from 2702 kg/h to 3328 kg/h, the reduced conversion ratio of fixed carbon also significantly decreased the calorific value of fuel gas from 4651 kJ/Nm^3 to 2697 kJ/Nm^3. Reactions R5 and R6 are both inhibited, and the CO concentration is more obviously affected. The CO concentration decreased from 10.41% to 4.20%, while the H_2 concentration was not obviously affected, ranging from 4.78% to 5.57%. Due to the decomposition of the raw meal, the components of the fuel gas changed significantly compared to those in the case without the raw meal, and the CO_2 concentration increased significantly from 12.46% in Case 1 to 30.61% in Case 3, which also affected the concentration of the remaining components.

4.5. Effect of the tertiary air temperature

As is shown in Fig. 10, after the temperature of the tertiary air

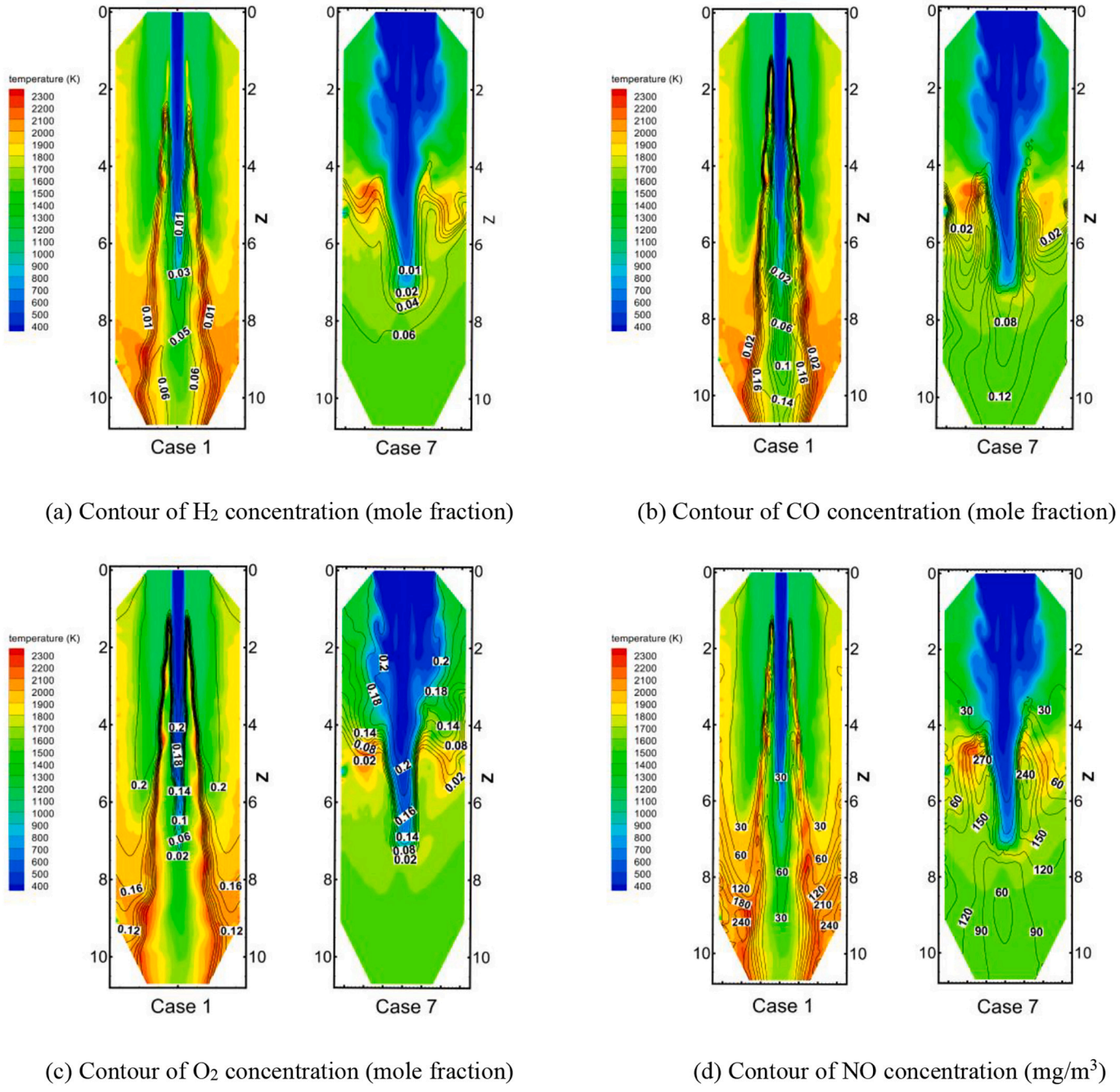

Fig. 10. Contours of gas composition depicted on the field of temperatures for Case 1 and Case 7.

increased from high temperature to room temperature, the temperature lower than 800 K in Case 7 increased dramatically, which delayed the pyrolysis of volatiles and the conversion of fixed carbon. At a distance of approximately 7 m along the gasifier, the low-temperature depths in the central region are similar, indicating that the thrust of the primary air is similar, while the lateral range is greatly expanded. Low-temperature tertiary air increases the time required for pulverized coal preheating and affects volatile fraction pyrolysis and the conversion of fixed carbon. When the zone near the wall meets the temperature required for the pyrolysis of volatiles, the reaction begins to accelerate. It can be seen from the contour data of the O_2 concentration that the velocity of the tertiary air is greatly reduced when the temperature changes to room temperature in Case 7, so the preheating time of the pulverized coal is prolonged and is sufficient for the exothermic reactions in Case 1. A high-temperature zone is formed in the middle of the gasifier, and the O_2 consumption rate is faster in this region. Compared to the high-temperature zone in Case 1, which is formed near the bottom outlet, the high-temperature zone in Case 7 effectively protects the inner material from thermal damage.

The temperature peaks are close to each other in the two cases, and the maximum NO concentration is 270 mg/m^3. However, because the sensible heat introduced into the gasifier by the tertiary air is greatly reduced in Case 7, the region of the high-temperature zone is significantly reduced; therefore, the concentration of NO at the outlet is reduced from 109 mg/m^3 in Case 1 to 90 mg/m^3 in Case 7.

The low temperature around the inlet delays the pyrolysis of volatiles and the conversion of fixed carbon in Case 7, and the O_2 consumption in the central area is slower than that in Case 1, resulting in lower rates of H_2 and CO generation. When the zone near the wall meets the temperature required for the pyrolysis of volatiles, the reaction begins to accelerate, resulting in a rapid increase in the concentrations of H_2 and CO. The H_2 concentration reaches 6% at a distance of approximately 8 m along the gasifier in Case 7, which is higher and more evenly distributed than that of 5% in Case 1. The CO concentration reaches 8% at a distance of approximately 8 m along the gasifier in Case 7, which is higher and more evenly distributed than that of 6% in Case 1.

A comparison between Case 1 and Case 7 shows that the higher the temperature in the gasifier is, the more the exothermic reaction is suppressed and the more the adsorption reaction is carried out completely. The concentrations of CO and H_2 both increased. The concentration of CO increased from 10.41% to 13.77%, and the concentration of H_2 increased from 4.78% to 6.24%, which both significantly increased the calorific value of the fuel gas from 4651 kJ/Nm^3 to 5348 kJ/Nm^3. The conversion ratio of fixed carbon increased from 49.15% to 55.01%, and the unreacted fixed carbon flow rate decreased from 2702 kg/h to 2392 kg/h. A decrease in the tertiary air temperature reduces the total enthalpy; thus, the temperature at the outlet decreases from 1927 K to 1565 K under a similar reaction process.

5. Conclusion

(1) Pulverized coal gasification using high-temperature tertiary air in a gasifier was simulated, and the results were compared with the experimental data. The feasibility of the model and the reliability of the algorithm were verified.
(2) The temperatures at the outlet decrease from 1927 K to 1563 K by the reduction of excess air coefficient, to 1831 K by the addition of steam, to 1349 K by the addition of raw meal. Those means can all be used to control the temperature in the gasifier and the addition of raw meal shows a better effect.
(3) The reduction of excess air coefficient leads to a higher concentration of CO and H_2, and fewer fixed carbon is reacted; the addition of raw meal depresses the generation of CO and H_2, and fewer fixed carbon is reacted; the addition of steam increases the concentration of CO and H_2, and more fixed carbon is reacted when compared to fundamental condition.
(4) The concentrations of NO at the outlet were 109, 98, 75, 91, 87, 76, and 90 mg/m^3 separately in 7 conditions. These values are significantly lower than those of complete combustion.

CRediT authorship contribution statement

Zhang Leyu: Writing – original draft, Visualization, Validation, Investigation, Formal analysis. **Chen Qingqing:** Writing – original draft, Validation, Investigation. **Wei Xiaolin:** Writing – review & editing, Supervision, Project administration, Investigation, Funding acquisition, Conceptualization. **Cheng Heng:** Resources, Project administration, Investigation. **Li Sen:** Project administration, Conceptualization.

Declaration of competing interest

The authors declare that they have no known competing financial interests or personal relationships that could have appeared to influence the work reported in this paper.

Data availability

Data will be made available on request.

Acknowledgments

This research is supported by the State Key Research & Development Program (Project No. 2016YFB0601503) and Jilin Province and the Chinese Academy of Sciences High-tech Industrialization Special Program for Science and Technology Cooperation (2024SYHZ0043), and the massively parallel computing is supported by the Tianhe II supercomputer.

References

[1] N.A. Madlool, R. Saidur, M.S. Hossain, N.A. Rahim, A critical review on energy use and savings in the cement industries, Renew. Sust. Energ. Rev. 15 (2011) 2042–2060.
[2] W.P. Adamczyk, S. Werle, A. Ryfa, Application of the computational method for predicting NO_x reduction within large scale coal-fired boiler, Appl. Therm. Eng. 73 (2014) 343–350.
[3] D.L. Baulch, C.T. Bowman, C.J. Cobos, R.A. Cox, T. Just, J.A. Kerr, M.J. Pilling, D. Stocker, J. Troe, W. Tsang, R.W. Walker, J. Warnatz, Evaluated kinetic data for combustion modeling: Supplement II, J. Phys. Chem. Ref. Data Monogr. 34 (2005) 757–1397.
[4] J.J. Li, M. Zhang, H.R. Yang, J.F. Lu, X.X. Zhao, J.C. Zhang, The theory and practice of NO_x emission control for circulating fluidized bed boilers based on the re-specification of the fluidization state, Fuel Process. Technol. 150 (2016) 88–93.
[5] H. Liu, Y.H. Liu, G.Z. Yi, L. Nie, D.F. Che, Effects of air staging conditions on the combustion and NO_x emission characteristics in a 600 MW wall fired utility boiler using lean coal, Energ, Fuel 27 (2013) 5831–5840.
[6] S.L. Fu, Q. Song, Q. Yao, Study on the catalysis of $CaCO_3$ in the SNCR deNO_x process for cement kilns, Chem. Eng. J. 262 (2015) 9–17.
[7] S.Y. Liu, B.Y. Wang, Z.X. Guo, B.Y. Wang, Z.H. Zhang, X. Ma, C.T. Chang, P. Wang, X. He, X.Y. Sun, S.J. Shuai, Experimental investigation of urea injection strategy for close-coupled SCR aftertreatment system to meet ultra-low NO_x emission regulation, Appl. Therm. Eng. 205 (2022) 117994.
[8] J. Mularski, H. Pawlak-Kruczek, N. Modlinski, A review of recent studies of the CFD modelling of coal gasification in entrained flow gasifiers, covering devolatilization, gas-phase reactions, surface reactions, models and kinetics, Fuel 271 (2020) 2326–2361.
[9] W.Y. Fan, T.L. Zhu, Y.F. Sun, D. Lv, Effects of gas compositions on NO_x reduction by selective non-catalytic reduction with ammonia in a simulated cement precalciner atmosphere, Chemosphere 113 (2014) 182–187.
[10] Z. Hu, J. Lu, L. Huang, S. Wang, Numerical simulation study on gas-solid two-phase flow in precalciner, Commun. Nonlinear Sci. 11 (2006) 440–451.
[11] J. Zhao, X.L. Wei, S. Li, R.N. Kang, Effect of equivalence ratio on gasification characteristics in a straw updraft gasifier, Proc. CSEE 37 (2017) 118–122.
[12] G.L. Song, Q.G. Lv, Q. Liu, Y.J. Na, Experimental research on coal gasification characteristics in single and dual circulating fluidized beds, Proc. CSEE 29 (2009) 24–29.
[13] Z.W. Yang, Z. Wang, Y.X. Wu, Z. Li, W.D. Ni, Use of a reactor network model in the design and operation of a new type of membrane wall entrained flow gasifier, Energy Fuel 27 (2013) 6322–6332.
[14] H.L. Wang, R.X. Bi, Achieving ultra-low NO_x emissions technology by combining Pyroclon Redox denitration gasifier with SNCR, Cement 7 (2022) 13–15.

[15] S. Li, L.C. Sun, X.L. Wei, Y.F. Ge, A high temperature tertiary air gasification and reburning system for efficient denitration in cement precalciner, Chinese Patent CN 107099336 B, August 29 (2017).
[16] C.T. Shi, J. Cai, Q.Q. Ren, H.X. Wu, H.J. Ma, Research progress of low NO_x emission control technologies in coal-fired cement kilns, Clean Coal Technol. 26 (2020) 174–183.
[17] M.A. Gómez, J. Porteiro, D. de la Cuesta, D. Patiño, J.L. Míguez, Numerical simulation of the combustion process of a pellet-drop-feed boiler, Fuel 184 (2016) 987–999.
[18] W.A. Fiveland, A.S. Jamaluddin, Three-dimensional spectral radiative heat transfer solutions by the discrete-ordinates method, J. Thermophys. Heat Trans. 5 (1991) 335–339.
[19] T.F. Smith, Z.F. Shen, J.N. Friedman, Evaluation of coefficients for the weighted sum of gray gases model, J Heat Trans-T Asme 104 (1982) 602–608.
[20] H. Kobayashi, J.B. Howard, A.F. Sarofim, Coal devolatilization at high temperatures, in: 16th Symp. (Int'l.) on Combustion, 1977, pp. 411–425.
[21] J. Andersen, C.L. Rasmussen, T. Giselsson, P. Glarborg, Global combustion mechanisms for use in CFD modeling under oxy-fuel conditions, Energy Fuel 23 (2009) 1379–1389.
[22] W.P. Jones, R.P. Lindstedt, Global reaction schemes for hydrocarbon combustion, Combust. Flame 73 (1988) 233–249.
[23] M.A. Field, Rate of combustion of size-graded fractions of char from a low-rank coal between 1200 degrees K and 2000 degrees K, Combust. Flame 13 (1969) 237–252.
[24] D. Toporov, P. Bocian, P. Heil, A. Kellermann, H. Stadler, S. Tschunko, M. Förster, R. Kneer, Detailed investigation of a pulverized fuel swirl flame in CO_2/O_2 atmosphere, Combust. Flame 155 (2008) 605–618.
[25] E. Desroches-Ducarne, E. Marty, G. Martin, L. Delfosse, Co-combustion of coal and municipal solid waste in a circulating fluidized bed, Fuel 77 (1998) 1311–1315.
[26] C.O. Sorensen, J.E. Johnsson, A. Jensen, Reduction of NO over wheat straw char, Energy Fuel 15 (2001) 1359–1368.
[27] D.L. Baulch, D.D. Drysdall, D.G. Horne, A.C. Lloyd, Evaluated kinetic data for high temperature reactions, J. Mol. Struct. 15 (1973) 169–170.
[28] R.K. Hanson, S. Salimian, Survey of rate constants in H/N/O systems, Comb. Chem. (1984) 361–421.
[29] G.G. De Soete, Overall reaction rates of NO and formation from fuel nitrogen, in: 15th Symp. (Int'l.) on Combustion, 1975, pp. 1093–1102.
[30] P.C. Malte, D.T. Pratt, Measurement of atomic oxygen and nitrogen oxides in jet-stirred combustion, in: 15th Symp. (Int'l.) on Combustion, 1975, pp. 1061–1070.
[31] R.H. Borgwardt, Calcination kinetics and surface area of dispersed limestone particles, AICHE J. 31 (1985) 103–111.
[32] J.J. Cai, L.Y. Wang, M.J. Li, Z.Z. Zhao, Experimental investigation on high temperature air coal gasification, Chin. J. Process. Eng. 8 (2008) 914–919.
[33] L.Y. Zhang, X.L. Wei, S. Li, Y.H. Zhai, Numerical simulation of O_2/CO_2 combustion in large cement precalciner, Sci. Sin. Technol. 49 (2019) 1080–1088.